MISR Cloud Detection over Ice and Snow Based on Linear Correlation Matching

Tao Shi *, Bin Yu †, and Amy Braverman ‡

Abstract

Cloud detection is a crucial step in any climate modelling or prediction. Multi-angle Imaging SpectroRadiometer (MISR) was launched in 1999 by NASA to provide 9 angle and 4 band data to retrieve or estimate the cloud height and hence cloud detection. However, cloud detection even with MISR data has been proven very difficult over ice and snow. In this paper, we bypass the cloud height estimation step to directly tackle cloud detection by using features of ice and snow (no cloud) pixels from different MISR angles. We propose the linear correlation matching classification (LCMC) algorithm based on Fisher linear correlation tests. We compare LCMC with the Steroscopically-Derived Cloud Mask (SDCM), which is the cloud mask from MISR Level 2 Top-of-the atmosphere Cloud algorithm (known as L2TC), and find that LCMC gives more coverage and more robust results judged by visual inspection of finer resolution images. LCMC can also detect the very thin clouds most of the time. Moreover, LCMC is computationally much faster than L2TC and easier to implement. We hope to combine LCMC with L2TC in the future to improve the accuracy of the L2TC cloud height retrieval.

Index Terms — Cloud detection, ice and snow, Multi-angle Imaging SpectroRadiometer (MISR), linear correlation.

1 Introduction

MISR was built for NASA by the Jet Propulsion Laboratory (JPL) in Pasadena, California, and is one of five instruments launched into polar orbit aboard NASA's Terra spacecraft in December 1999. MISR is part of NASA's Earth Observing System (EOS) program, which was conceived to provide data for in-depth scientific investigations of Earth's processes as a unified system. These data facilitate studies of critical processes such as global warming and greenhouse effects.

Clouds play a major role in Earth's climate by differentially warming and cooling the Earth. It is widely acknowledged that clouds introduce uncertainties in radiative feedback to the climate system,

*Department of Statistics, University of California, Berkeley, CA 94720-3860. Email: taoshi@stat.berkeley.edu
†Department of Statistics, University of California, Berkeley, CA 94720-3860. Email: binyu@stat.berkeley.edu
‡Jet Propulsion Laboratory, California Institute of Technology, Pasadena, CA 91109-8099.
Email: Amy.Braverman@jpl.nasa.gov
** Revised September 2003.

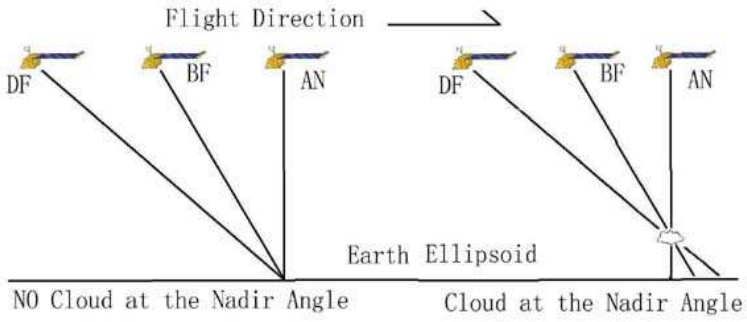

Figure 1: MISR data registration. Only three of the nine angles are shown here (An (nadir), Bf (45.6° forward) and Df (70.5° forward)).

and that this poses a most formidable obstacle to climate prediction and weather forecasting. In particular, in polar regions where scenes are dominated by ice and snow, the net radiative impact is hard to discern (Diner et al, 1999a; Charlock and Ramanathan, 1985; Li and Leighton, 1991). Some studies indicate that clouds tend to warm the surface-atmosphere system over highly reflective surfaces (Stephens et al, 1981; Nakamura and Oort, 1988), but others studies suggest clouds have a net cooling effect (Li and Leighton, 1991; Schweiger and Key, 1994). Moreover, most aerosols are bright particles that reflect sunlight back to space. They tend to cool the surface by reducing the amount of solar radiation absorbed at the surface. Aerosol information cannot be retrieved in the presence of clouds, so good cloud identification methods are essential for aerosol studies. The ability to detect clouds in the polar regions is therefore critical to understanding Earth's radiation budget, and the role of clouds in the climate system.

The MISR instrument offers a new and promising avenue for cloud detection methods. MISR has nine cameras looking at the Earth from different angles simultaneously. The nine camera angles are 70.5°, 60°, 45.6°, 26.1° forward, nadir and 26.1°, 45.6°, 60°, 70.5° afterward (referred to as Df, Cf, Bf, Af, An, Aa, Ba, Ca, Da, respectively). Each angle has four observing bands (red, green, blue, and near-infrared). The spatial resolution is 275m by 275m in red band and in all bands of the An camera, and 1.1 km by 1.1 km in green, blue, and near-infrared bands of the off-nadir cameras. The instrument about produces six million measurements per orbit with 16 orbits per day (Muller et al, 2002). This multi-angle information permits direct retrieval of cloud heights, which is impossible using single angle views (Diner et al, 1999a). MISR registers each pixel to the Earth's surface ellipsoid. The higher an object is, the greater the disparity between its ellipsoid-projected positions as seen from different angles. Fig. 1 shows the registration for three of nine MISR cameras (Df, Bf and An). Simple trigonometry allows one to determine cloud height, and height can then be thresholded to determine whether a cloud is present or not. This is the basis of the the MISR cloud height retrieval algorithm (L2TC) and the Steroscopically-Derived Cloud Mask (SDCM). It works well in many cases, but fails to classify a substantial portion of pixels correctly when applied over ice and snow scenes because it is difficult to identify matching pixels in different views against the bright background.

Fig. 2 displays an RGB image of the An view over the East Siberian Sea, Russia, obtained on July 24, 2002 (MISR orbit 12986, blocks 22-24). The left panel is at 1.1km by 1.1km resolution,

while the right panel is at 275m by 275m resolution for the middle sized, boxed region in the left panel. It is almost impossible to identify clouds in the 1.1km by 1.1km image by visual inspection. The algorithms do find clouds which can be confirmed looking at the finer resolution in the right panel.

Recall that when a cloud is present, it is registered at different locations for images taken at different angles (cf. Fig. 1). The challenge of retrieving cloud height is thus that of matching the same cloud scene in images representing different angles. After matching at three non-symmetric angles, we can use angle, flight time, and geometry to solve for cloud motion and height. Matching over ice and snow is hard since the cloud textures are easily confused with those of ice and snow. Our LCMC method approaches the problem from another point of view. It is based on matching the ice and snow pixels when no clouds are present. This provides better speed and accuracy.

In section 2, we review briefly a few stereo matchers used in MISR's algorithms. We describe our LCMC algorithm in section 3. The comparision of LCMC with the MISR algorithms and an example of LCMC thin cloud detection are given in section 4. Section 5 concludes with a discussion and ideas for future work.

2 Review of Existing Algorithms

Here we review two algorithms that have been used or investigated by the MISR science team. The algorithm in use now is called MISR level 2 top-of-the atmosphere cloud algorithm (L2TC)(c.f. Dinner et al, 1999). Pyramidal Gruen-Otto-Chau adaptive least squares correlation matcher (P-Gotcha matcher) is another matcher that had been considered for MISR cloud height retrieval in JPL (c.f. Gruen, 1985; Otto and Chau, 1989; Holden et al, 1993).

2.1 L2TC Cloud Height Retrieval Algorithm

L2TC uses Df-Bf-An-Ba-Da cameras for cloud top motion retrieval (estimation) and uses Af-An-Aa cameras for cloud height retrieval (estimation). First the top cloud motion is estimated or retrieved and it is used to estimate or retrieve the cloud height. Thresholding the cloud height gives the cloud mask, Steroscopically-Derived Cloud Mask (SDCM).

Raw MISR measurements are transformed into Bi-directional Reflectance Factors (BRF's), i.e. the ratio of observed radiance at a particular illumination and view geometry and the radiance that would be obtained under the same conditions with a target consisting of a perfect lambertian reflector (cf. Diner et al, 1999b). The 275m resolution red band is used, because it provides high resolution data. However, the classification label is given only at 1.1km resolution to reduce computation. (In this paper, we concentrate mainly on the red band for the same reason, but would like to investigate the use of other bands for further improvements in the future.)

L2TC estimates cloud motion and height in two separate stages, although they can be solved with two linear equations simultaneously after a match is found. This choice reflects a compromise between computational speed and classification accuracy. At the first stage L2TC retrieves the

cloud-top motion over non-overlapping blocks of size 70.4km × 70.4km for computational speed. It is not feasible to match every pixel in three angles at high resolution, especially for the most oblique angle (Df). Cloud movement in a 70.4km block is assumed constant, and in particular cloud vertical movement is assumed negligible during the 7-minute observation period. L2TC uses Nested Maxima Stereo-Matcher (NM) to find matching blocks using three cameras (An-Bf-Df). NM is a feature-based matcher designed to run through large amounts of data at high speed. A nested maximum is defined as a central pixel within a 5 pixel vertical column such that the BRF decrease monotonically in value for two pixels on both sides of the maximum pixel. L2TC first searches for all nested maxima in both the reference (Bf) angle image and the image to be searched in (An and Df); then it takes one maximum from the reference image and one maximum from the searched image to test if they match each other. For an 11 by 21 pixel patch (window) around each target pixel (maximum here), M2 and M3 (defined below) match metrics are calculated (Diner et al, 1999b) to decide on a match (empirically chosen thresholds 1 for M2 and 0.75 for M3). If there is no match, then a label "no retrieval" is given for the block and hence no pixels in the block will have cloud motion retrievals, or cloud height retrievals. Also, if there are too many matches in the block, cloud motion cannot be retrieved, and "no retrieval" is also given to such blocks.

The M2 metric is defined as:

$$S_{M2} = \frac{\sum_{i,j} |[\frac{R(x_i,y_j)-\bar{R}}{R_{max}-R_{min}}] - [\frac{C(x_i,y_j)-\bar{C}}{C_{max}-C_{min}}]|}{\sigma_{M2}} \tag{1}$$

with

$$\sigma_{M2} = \sum_{i,j} |[\frac{R(x_i,y_j)-\bar{R}}{R_{max}-R_{min}}]| \tag{2}$$

where $R(x_i, y_j)$ is the reference pixel BRF at (i, j); $C(x_i, y_j)$ is the corresponding value in the comparison image; R_{max}, R_{min} are the maximum and minimum values within the reference patch, respectively; C_{max}, C_{min} are the maximum and minimum values within the comparison patch, respectively; $\bar{R}$ is the average value within the reference patch; $\bar{C}$ is average value within the comparison patch. M3 uses medians rather than means to define a metric in a similar way (cf. Diner et al, 1999b).

After a match is found, L2TC uses the following equations to determine cloud motion, even though cloud height is obtained at the same time by solving these equations:

$$v_c(t_{An} - t_{Bf}) - h(tan(\theta_{Bf}) - tan(\theta_{An})) = (x_{An} - x_{Bf}) \tag{3}$$

$$v_c(t_{Df} - t_{Bf}) - h(tan(\theta_{Bf}) - tan(\theta_{Df})) = (x_{Df} - x_{Bf}) \tag{4}$$

where v_c is the along-track cloud movement speed (cloud motion); h is the cloud-top height; t is the time when the given camera looks at that location; θ is the angle of view direction and the zenith; $x_{An} - x_{Bf}$ and $x_{Df} - x_{Bf}$ are the along-track location shifts of the best matched patch in An vs. Bf and Df vs. Bf.

At the second stage of L2TC, cloud-top motion, v_c, for the block is assumed known, and the An and Af images are used to obtain cloud height on a pixel-by-pixel basis. L2TC finds the match in An/Af angles and solves just one linear equation (3) to get cloud height, if we replace B_f by A_f and use the cloud movement speed v_c got from the first stage.

M2 and M3 are also used to retrieve the cloud height pixel by pixel. L2TC calculates the M2 metric of a small pixel patch (e.g. 6 by 10) extracted around the target pixel chosen for matching, and a patch around each comparison pixel in the search window. The pair of patches with the lowest metric value is chosen. The match must pass both the threshold test (e.g. M2 metric less than threshold) and ambiguity tests (e.g. metrics at other locations in the search window are larger than 110% of the metric at the best match) to be accepted. For a successful M2 match, M3 is applied to this best matching location to determine whether M3 verifies the point as valid match. If a match can not be found, cloud height for that pixel is labelled as "no retrieval". (The thresholds for M2 and M3 are derived empirically by studying match quality versus metric value for a number of different scenes. The relationship does not vary with scene type, and are specific to all MISR scenes, irrespective of the types of clouds present in the scene.) L2TC detects cloud by thresholding the difference of cloud height estimation and terrain height, so there is no cloud detection result for the cloud height "no retrieval" pixel.

The main drawback of L2TC over is that cloud height retrieval fails for an entire block when the NM matcher fails. This happens particularly over ice and snow, because the local maxima of the BRF's from cloud and ice/snow are mixed up. When the cloud motion for a block are retrieved successfully, M2 and M3 sometimes also fail to find matches in the second step. The right panel of Fig. 3 shows the "no retrieval" pixels from L2TC, in which cloud motion is retrieved successfully for all the blocks. It fails on 18% of pixels. The blockiness (70.4×70.4 km^2) in the motion retrievals leads to blockiness in the height retrievals as well.

2.2 P-Gotcha Matcher

The P-Gotcha matcher is based on a parametric regression model, refitted at candidate matching pixels sequentially. It assumes smooth reflectance and terrain surfaces. Hence, a linear Taylor approximation can be made locally and gives a local, linear regression model. The fitted parameters give the location coordinates of the next candidate matching pixel relative to the location of the current candidate. The process stops when parameters fall below a threshold, or the candidate matching pixel becomes stable.

P-Gotcha was originally selected as the stereo-matcher for MISR because it provides sub-pixel acuity by interpolation in the parametric model (typically to 0.3 pixels), and can provide a precision matrix for estimating accuracy. However, P-Gotcha is exceedingly slow since it performs least-squares fitting at every candidate matching pixel (about 10^5 floating-point operations per match, Muller et al, 2002). Empirically it was found that searches started more than 3 pixels away from the best match do not converge, so the coverage is also promising. The MISR team decided not to proceed with this algorithm as the operational matcher even using a parallel implementation. However, when it does converge, P-Gotcha provides a benchmark by which to judge the performance of other algorithms.

In summary, over ice and snow neither L2TC nor P-Gotcha provide good coverage. Cloud detection in polar regions remains an impediment to making full use of MISR multi-angle capabilities in this area.

3 Linear Correlation Matching Classification (LCMC)

We propose a new algorithm, the Linear Correlation Matching classification (LCMC) algorithm. This algorithm can be used for classification of clear pixels over ice (hence also cloud pixels by exclusion).

3.1 Rational Behind LCMC

The rationale behind LCMC is as follows. Since the radiances into different cameras (angles) at a particular band from the same scenery are approximately proportional to the intensity of the light source (sun), they should be strongly correlated. Over ice and snow, the radiances are relatively high and this correlation is obvious. (In contrast, the radiances of clear sea pixels are very low, so the correlation is masked by random noise.)

Preliminary data analysis via scatter plots on the MISR data confirms the strong correlation. Examples of such scatter plots are displayed in Fig. 4 for the smallest windows in the left image of Fig. 2 with the 1.1km by 1.1km resolution. The upper left plots correspond to the upper smallest window in Fig. 2 and show a strong linear correlation of radiances between Bf and Df in red band. When there is no cloud or the cloud does not change too much in the 7 minutes observation period, the best match corresponds to a very high linear correlation over a small search area. Next we describe our LCMC algorithm.

3.2 LCMC Algorithm

We use the earth surface ellipsoid projected data. The proposed method works for any three non-symmetric angles. To be concrete, we will describe it using the An, Bf and Df angles. This angle combination also provides the best cloud height separation among all forward angles (Diner et al, 1999b). (An, Ba and Da angles are reserved to validate the result.)

A small patch (9 by 9 pixels) is chosen centered at the pixel to be classified, using Bf angle as the reference angle, An and DF angle as comparison angles. If there is no cloud over that location from all three angle we used, and the terrain height is not too high from the earth surface ellipsoid, the linear correlation coefficient r between radiances in the An patch and the Bf patch at same location should be very strong. If we move the center of the Bf patch one pixel forward or backward along the flying direction, the strong linear correlation will be destroyed. This observation holds also between Bf and Df, see the upper two panels in Fig. 4. From equation (3) and(4), the camera angles, flying time, and geometry show that the cloud can not be registered at the same location in An, Bf and Df angles at the same time (cf. Diner et al, 1999b). So if there is cloud over the window, the An/Bf and Bf/Df linear correlations at the same location will not be much stronger than one pixel forward or backward, see the lower two panels in Fig. 4.

We build the LCMC classification rule based on this observation. We calculate the linear correlation coefficients of the Bf (reference angle) patch with An (comparison angle) patches one pixel forward (r_{B_f}), same location (r_{B_s}), and one pixel backward (r_{B_b}) respectively. We test if the

same location correlation coefficient r_{B_s} is greater than other two significantly. The test is Fisher's linear correlation test (Fisher, 1925). We transform all three r to $z = \frac{1}{2}\log((1+r)/(1-r))$. If the data vectors are *i.i.d.* and follow jointly a Gaussian distribution with correlation ρ, z approximately follows normal distribution with mean $\frac{1}{2}log((1+\rho)/(1-\rho))$, variance $1/(n-3)$ (here $n = 81$). The scatter plots show that this joint Gaussian assumption holds approximately for our data. (We ignore the dependence between the pixels in the same small patch as a first approximation.)

For the Bf and An angles testes, we use the 5% level to test the null hypotheses $\rho_{B_s} \leq \rho_{B_f}$ and $\rho_{B_s} \leq \rho_{B_b}$. They are rejected when data fall into rejection regions, i.e., $\{z_{B_s} - z_{B_f} > 1.645\sqrt{2/(81-3)}\}$ and $\{z_{B_s} - z_{B_b} > 1.645\sqrt{2/(81-3)}\}$. We carry out the same testes for Bf and Df angles. A clear (no cloud) pixel is declared if all four null hypotheses are rejected, otherwise cloudy.

3.3 Computational Order of LCMC

The computation of LCMC is much simpler than L2TC and P-gotcha, since LCMC only calculates six correlation coefficients to classify each pixel. It is linear in the number of pixels processed. We need not go through a search window to find the best match, which is the most expensive part of the other algorithms. Matching the ground, instead of the cloud, provides us such advantages. By design it also has a 100% coverage.

3.4 Angle and Cut-off Points Selection

Since there are more angles to be used for this testing, in the future we plan to explore approaches to combine the tests (e.g. multiple testing) to set the cut-off values for cloud detection. The cut-off value might vary according to the pair of angles used in the test since the angles near An provide more reliable information than those away from An because they incur smaller time differences when observing the same scene. In addition, we would also like to explore the possibility of using the other three bands to improve cloud detection based on the red band.

By introducing the statistical testing idea into the model, we want to investigate the confidence levels associated with the matching result. We hope to find a way to access the confidence levels of the classification results along this direction. We need "ground truth" from other resources to work with.

4 Experimental Results of LCMC

A case study is carried out to compare LCMC with SDCM. The East Siberian Sea data (An angle RGB image in Figure 2) is used. Since the Df angle does not cover the area outside of the big window in the image, we constrain our comparisons inside of the window. The second example shows the ability of LCMC to detect the very thin cloud over ice and snow.

4.1 Comparisons Between LCMC and SDCM

As described in L2TC review section, the SDCM classification algorithm takes as input the 275m by 275m resolution data (red band) and outputs classification labels at the 1.1km by 1.1km resolution. Because of time constraint, we applied the LCMC classification algorithm only to the 1.1km by 1.1km resolution data (red band as well), and obtained classification labels also for the 1.1km by 1.1km resolution. A 288 by 361 pixel sub-image in Fig. 2 (indicated by the largest box in the left panel) was chosen so that L2TC gave cloud motion retrievals for all pixels to simplify the matter. But the matching in the height retrieval of L2TC failed at 18% of the pixels. LCMC classified all pixels by design. Table 1 contains the comparisons. For LCMC no cloud or clear pixels, LCMC and SDCM agree 86.5% of the time, disagree 0.65% of the time, and 12.8% of the time, L2TC has no retrieval.

	SDCM No Cloud	SDCM Cloudy	SDCM Not Retrieved	Total
LCMC No Cloud	27.86%	0.21%	4.12%	32.2%
LCMC Cloudy	35.22%	18.4%	14.18%	67.8%
Total	63.08%	18.61%	18.31%	100%

Table 1: Comparing the LCMC result with SDCM.

We investigated the pixels not classified by L2TC (18%) in the small boxed windows in the left image of Fig. 2 – we zoomed in to the 275m by 275m resolution to get the right image of Fig. 2. Cloud and ice can now be distinguished by eye at this resolution, but not very easily. The left panel of Fig. 3 shows the LCMC classification result of the data in Fig. 2 ("No cloud" pixels are coded as white points in the picture, and "cloud" pixels are left in the true color). The white points in the right panel of Fig. 3 are the pixels Where L2TC failed. For the L2TC unclassified pixels, LCMC seems to give reasonable results. Future validation has to be made based on other sources.

The scatter plots of radiances of the 9 by 9 windows in Bf/Df angles are shown in Fig. 4. The upper two plots are from the upper smallest window in Fig. 2, which is classified as "no cloud" by LCMC. The linear correlation coefficient drops sharply when we moved the Df window one pixel forward. The lower two plots are from the lower smallest window in Fig.2, which is labelled as "cloudy" by LCMC classification. The linear correlation gets stronger when we move Df window one pixel forward. So the evidence is strong for LCMC to classify a pixel as "no cloud".

The largest disagreement of LCMC and L2TC occurs in the category of LCMC cloudy and L2TC no cloud. This is due to the fact that the LCMC classifies one pixel as "no cloud" when there are no clouds over the 9 by 9 window at all the three angles (An, Bf and Df), that is, it does not classify the pixel as "no cloud" based only on the An/Af pair. However, such pixels are most likely classified as "no cloud" by L2TC, because it uses only the An/Af pair to do the cloud height retrieval. So it is possible to improve accuracy of the L2TC by using other angles, but at the price of a larger searching window. The accurate detection of "no cloud" or clear pixels by LCMC is important in its own right because the MISR aerosol retrieval algorithm needs to know where the clear or no cloud pixels are.

4.2 Comparing LCMC with Expert Labelled Data

We also use 400 expert labelled pixels to test both LCMC and SDCM. They are from MISR orbit 12986, block 22-24 (c.f. Fig. 2). The 400 pixels are labelled by visual inspection on the 275m resolution data. "No cloud" pixels are chosen from the top middle or middle left area of the image, while "cloudy" pixels are from the top left and bottom left of the image. 200 clear pixels and 200 cloudy ones are include in the test. All test pixels are from areas where it is easy to separate"cloud" or "no cloud". The test results are given in Table 2.

Mis classification Rate	No Cloud	Cloudy	Total
LCMC	47.5%	0%	23.75%
SDCM	42%	28%	35%

Table 2: Mis classification rates of LCMC and SDCM.

We notice that we use 1.1km by 1.1km resolution data in LCMC algorithm, but SDCM is derived based on the 275m by 275m resolution. Our algorithm still provides 12% improvement over all. The results show again that the LCMC is very good at picking up high clouds. It makes very few mistakes when there are really clouds above a certain height. Over the"no cloud" area, the LCMC gives comparable result as SDCM, and both algorithms have relatively high mis classification rates. One reason for this mis classification is that we use the ellipsoid projected data in the LCMC algorithm. The high terrain surface will be registered in different locations, so the LCMC algorithm fails to pick it up when no cloud presents. We plan to test LCMC on the MISR terrain projected data to see possible improvement. In the next stage, we also plan to test the LCMC on the 275m by 275m resolution data and hope it can find the very low cloud (below 1km) in the finer resolution.

4.3 Detecting High and Thin Cloud over Ice and Snow by LCMC

So far all the stereo matching algorithms assume no shape change of the clouds during the observation interval. Cloud shape change will make the problem much more difficult for the nested maximum (NM), M2 and M3 matchers to do their jobs. In contrast, the shape change does not present anything more difficult for LCMC because it relies on features of clear pixels which remain the same with or without the cloud shape change. So LCMC should work well in detecting high and thin cloud over ice and snow.

Fig. 5 displays a RGB image at the An angle of MISR orbit 2461 and block 28-31 and the LCMC result. The left panel is RGB picture with the 1.1km by 1.1km resolution, and the right panel is the LCMC result ("No cloud" is coded as bright points). The left upper part of the image is covered by high and thin cloud, it was detected by the LCMC algorithm very well. L2TC is not applied to this data, because the data was collected before L2TC started to be used. (The "no cloud" pixels over sea are not classified by LCMC, but by thresholding the Infrared radiances.)

5 Discussions and Future Work

In summary, LCMC classifies the pixel as "no cloud" when the evidence is strong. LCMC has full coverage to pick out the "no cloud" pixels. By design, LCMC algorithm relies mostly on the surface spatial information of the ice and snow surface. Other MISR bands can be used given there is enough energy in the bands reflected from the ground. We tested LCMC using green and blue bands on the MISR data shown in Fig. 2 and Fig. 5, and both bands provide very close classification results in our tests.

LCMC does not work over ocean because the linear correlation is masked by random noises, since radiance is very low. In this case, MISR's Level-1 cloud detection algorithm easily detects clear pixels over deep ocean, by thresholding the near infrared radiance. So we can simply threshold the near infrared band to exclude carrying out LCMC for that pixel.

LCMC can be used to preprocess data for L2TC cloud height retrievals. After we get high confidence "no cloud" pixels from LCMC, we could run L2TC only for the "cloud" pixels. In the L2TC cloud motion retrieval, we will then be more confident that we are matching clouds, not ice and snow surface features. Accuracy and speed are both improved in this step. For the L2TC cloud height retrieval, we do not need to search matching patches for the "no cloud" pixels. This reduces the computational burden and improves coverage.

High topography poses difficulties for LCMC because high altitude terrain will be registered at different locations for different view angles. We need to incorporate terrain height information into the LCMC algorithm. Since terrain height is provided by an external source, and MISR provides the terrain projected data, we are going to test the LCMC algorithm on terrain projected data in the next stage.

In the next step, we want to implement LCMC on the 275m by 275m resolution data. At this finer resolution we expect LCMC to provide better results, because high resolution provides more data for a much smaller window. Matching tests are carried out even more locally. When a pixel and its neighborhood are not coved by clouds, and there are clouds somewhere in the 9.9km by 9.9km window, the 275m by 275m resolution LCMC will pick this out while the 1.1km algorithm misses it. We also expect the finer resolution data will help us to find the low clouds. We would also like to experiment with selecting angles for use in the finer resolution scenario.

We will validate the LCMC result with the cloud classifications over snow and ice from other sources Reliable data from other source could also be used to improve selection of angles, bands, and window sizes. One source of validation data is the North Slope of Alaska Surface-Satellite Cloud Comparison Data Site [15]. It provides cloud microphysics data from a surface observation site (latitude=71.17 longitude=203.22) in Barrow, Alaska. It is operated by the Department of Energy, and its main purpose is to provide validation data for satellite cloud sensors, particularly those on the TERRA satellite. Clouds observed with sensors operating at this ARM North Slope of Alaska CART site have been classified based on subjective (human) examination of data from radar, microwave and infrared radiometers, and radiosondes.

Summary

As cited in Diner et al (2002), the 20th Century writer Zora Neale Hurston wrote: "There is no single face in nature, because every eye that looks upon it, sees it from its own angles." MISR looks at the Earth from nine different angles and provides us new ways to understand the changes taking place on our home planet. In this paper, we considered the problem of detecting clouds over ice and snow from a different point of view: matching the ground rather than the clouds. MISR's data collection method makes it possible to derive a fast algorithm for distinguishing clear ice and snow pixels from cloud-covered pixels. The algorithm also holds potential for detecting the thin cloud, even when the cloud shape changes. In the future, we hope to extend the method to work over other land scenes, and combine it with L2TC for further improvements.

Acknowledgements

Tao Shi is partially supported by NSF grant FD01-12731. Bin Yu is partially supported by NSF grant FD01-12731 and ARO grant DAAD19-01-1-0643. Amy Braverman's work is performed at the Jet Propulsion Laboratory, California Institute of Technology, under contract with the National Aeronautics and Space Administration. MISR data were obtained at the courtesy of the NASA Langley Research Center Atmospheric Sciences Data Center. The authors would like to thank D.J. Diner, R. Davies, R. Kahn, and L. Di Girolamo for helpful suggestions and discussions.

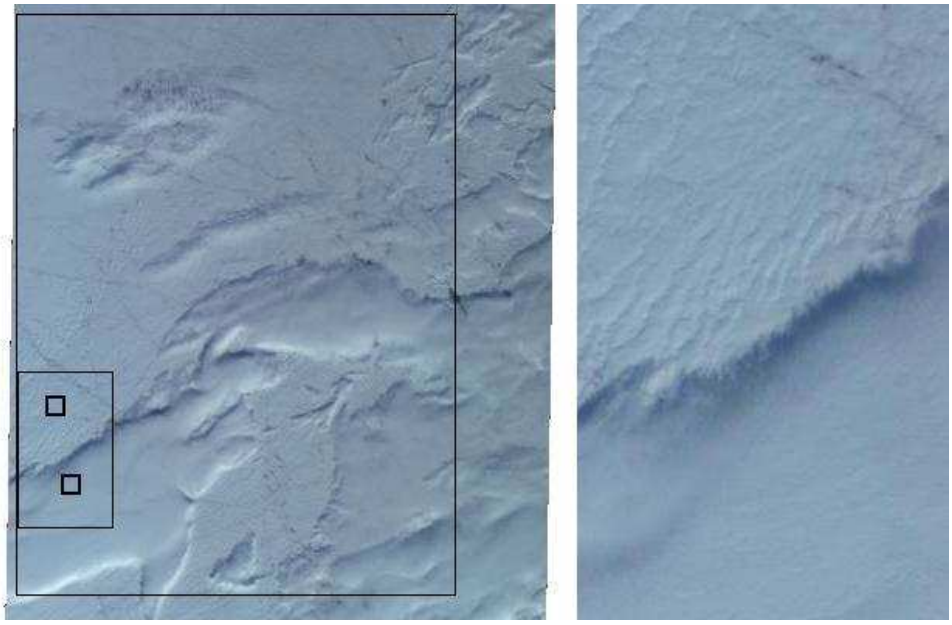

Figure 2: RGB true color image of the East Siberian Sea, Russia (obtained July 24, 2002). MISR orbit 12986, block 22-24, An angle. Left image: RGB in 1.1km by 1.1km resolution image; Right image: RGB 275m by 275m resolution image in the middle size window of the left image.

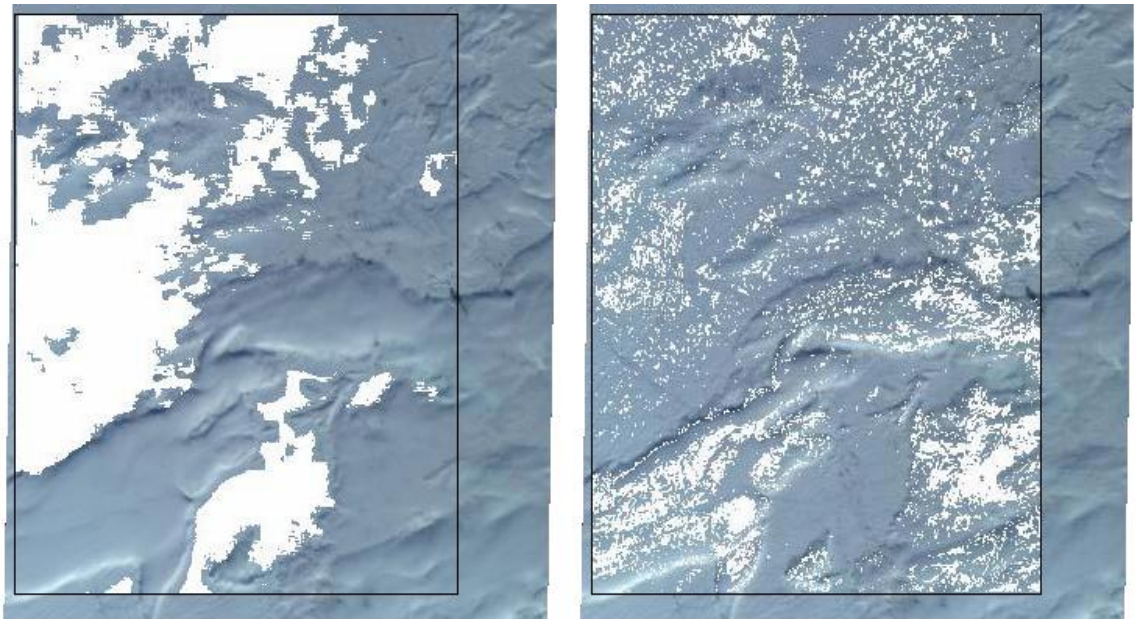

Figure 3: MISR Orbit 12986, block 22-24. The left panel is the LCMC result, with "no cloud" pixels coded as white points. The right panel highlights the L2TC failed pixels, coded as white points (The cloud motions are retrieved successfully for all 70.4km by 70.4km blocks.)

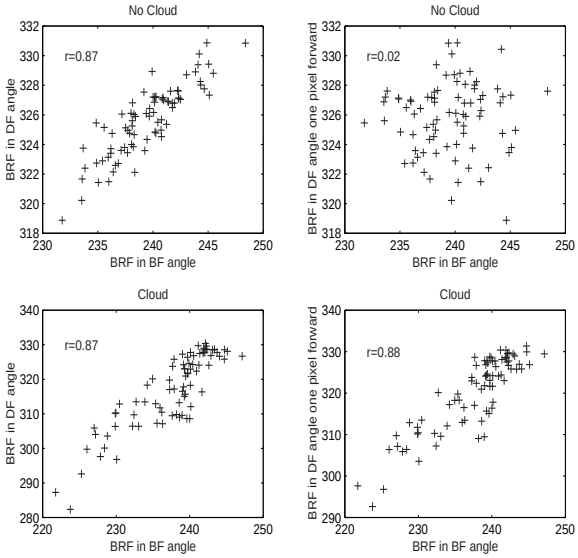

Figure 4: Scatter plots of the radiances from Fig. 2. The upper two plots are from the upper smallest window in Fig. 2: the left one plot is from BF and DF angles without moving the DF angle patch, and the right one with DF angle patch moved one pixel forward. The lower two plots are from the lower smallest window in Fig. 2: the left is the plot of radiances in the BF and DF angles without moving the DF angle patch, and and the right one with the DF angle patch moved one pixel forward.

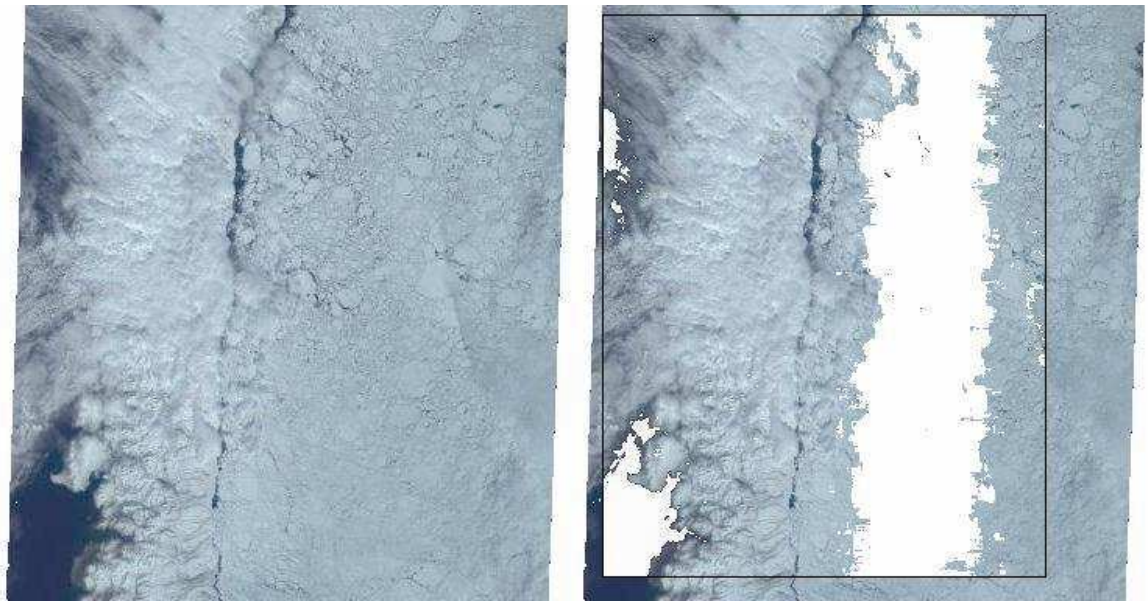

Figure 5: MISR Orbit 2461, block 28-31, AN angle. The left panel is the RGB true color picture, 1.1km by 1.1km resolution. The right panel is the LCMC cloud detection result, with "no cloud" coded as white points. The high thin cloud is detected by the algorithm.

References

[1] Charlock, T.P., and Ramanathan, V. (1985). The albedo file and cloud radiative forcing produced by a general circulation model with internally generated cloud optics. *J. Atmos. Sci.*, **42**, 1408–1429.

[2] Diner, D.J., Asner, G.P., Davies, R., Knyazikhin, Y., Muller, J. Nolin, A.W., Pinty, B., Schaaf, C.B., and Stroeve, J. (1999a). New directions in earth observing scientific applications of mulitangle remote sensing. *Bulletin of American Meteorological Society.* **80**, 2209–2228.

[3] Diner, D.J., Davies, R., Di Girolamo, L., Horvath, A. Moroney, C., Muller, J.-P., Paradise, S.R., Wenkert, D, and Zong, J. (1999b). MISR level 2 cloud detection and classification algorithm theoretical basis. Jet Propulsion Lab., Pasadena, CA, JPL Tech. Doc. D-11399, Rev. D, 1999.

[4] Diner, D.J., Verstraete, M.M., and Martonchik, J.V. (2002) Foreword to special section on MISR *IEEE Trans. Geosci. Res. Lett.* **40**. July, 1447–1448.

[5] Fisher, A. R. (1925). *Statistical methods for research workers*, Hafner Publishing Company.

[6] Gruen, W.A. (1985). Adaptive least squares correlation: A powerful image matching technique. *S. Afr. J. Photogramm., Remote Sens. Cartogr.* **14** 175–187.

[7] Holden, M, Zemerly, J.M. and Muller, P.J. (1993). Parallel stereo and motion estimation. in *Parallel Architectures and Algorithms for Computer Vision, Image Processing and Neural Networks.* I.pitas, Ed. Chichester, U.K.: Wiley. 175 –232.

[8] Moroney, C., Davies, R. and Muller, -P.J. (2002). Operational retrieval of cloud-top heights using MISR data. *IEEE Trans. Geosci. Res. Lett.* **40**. July, 1532–1540.

[9] Muller, -P.J., Madanayake, A., Davies, R., Diner, J.D., and Paradise, S. (2002). MISR stereoscopic image matchers: Techniques and results. *IEEE Trans. Geosci. Res. Lett.* **40**. July, 1547–1559.

[10] Nakamura, N. and Oort, H.A. (1988) Atmospheric heat budgets of the polar regions. *J. Geophys. Res.*, **93**, 1380–1395.

[11] Otto, P. G. and Chau, W. T. (1989). Region-growing algorithm for matching of terrain images. *Image Vision Computation* **7**, 83–94.

[12] Schweiger, A.J. and Key, R.J. (1994). Arctic Ocean radiative fluxes and cloud forcing estimated from the ISCCP C2 cloud dataset, 1983-1990. *J. Appl. Meteor.*, **33** 948–963.

[13] Stephens, G.L., Campbell, G.G. and Vonder Haar, H.T. (1981). Earth radiation budgets. *J.Geophys. Res.*, **86**, 9739–9760.

[14] North Slope of Alaska/Adjacent Arctic Ocean Site website. *http://www.arm.gov/docs/sites/nsa/nsaaao.html*